Microhardness of Polymers

Chapter 9. Microhardness of Polymers

9.1 Introduction

Microindentation involves deformation of a test material on a very small area ranging $(10^{-1}\sim10^{-2}mm)^2$, and provides information about micromechanical properties such as hardness, elastic modulus, creep compliance etc [1]. This technique was used in the study of microhardness of metals and ceramics for several decades and was proved to be sensitive to the chemical composition and microscopic structure of the materials [2,3]. Application of this technique to polymers was relatively new with development of the polymer science. During the last two decades, microindentation test appeared as a valuable tool to present morphology-property relationship of polymers [4-9]. This technique basically correlates to the anisotropy of hardness with the molecular orientation of polymers. Thus, the microhardness test in combination with the X-ray diffraction technique is extremely useful for morphological studies including crystallization of polymers [1,4,6].

Based on the above fact, microhardness measurements were performed in the oriented crystallization of PP and PET [7, 9]. This chapter aims to present details of the microhardness measurements including the indentation geometry, and the results are discussed with those obtained by the X-ray diffraction as presented in chapters 4 and 5.

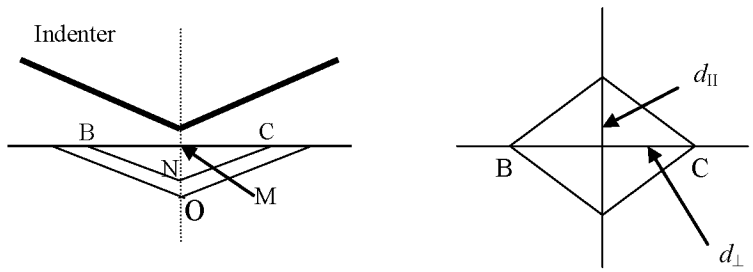

Fig. 9.1 (a) Side view of the indenter (b) Surface-view of the oriented film

9.2 Indentation geometry

Microhardness experiments are carried out at room temperature using a Leica Microsystems indentation equipment. As an indenter, a Vickers square-based diamond pyramid, with the top angle of 136°, is used. The indenter penetrates the surface of a sample upon the application of a given load at constant rate. Figure 9.1a illustrates a side view, representing the contact geometry of the indentation. The sample surface as pointed by M remains flat at a zero load. The position M is deformed to O upon loading due to a compressive pressure. On unloading, the deformation is yielded by an elastic recovery from

O to N. Then, a pattern of the plastic deformation is observed by the ultimate arrangement and organization of the molecules. As shown in Fig.9.1b, we measure the value of diagonal length d of the indentation pattern (imprint) on the sample surface.

Microhardness values, H, are calculated by the following equation;

$$H = k\,P/d^2\,, \qquad (9.1)$$

where P is the load applied, d is the measured diagonal of the residual imprint and k is a geometric constant. A value of k = 1.854 is used when P is in N and d in mm to give H in MPa. In the preliminary tests, the P/d^2 ratio was observed to be constant for different loads [1,4].

Depending on the sample category, whether it is amorphous or crystalline, isotropic or oriented, the surface view of the imprint will have different shapes. The imprint of the oriented sample usually reveals a lozenge shape as shown in Fig.9.1b. We measure both diagonal lengths, $d_\perp$ and d_{II}, perpendicular and parallel to the oriented direction, respectively. Then the hardness values, $H_\perp$ and H_{II} , are calculated by Eq. (9.1). In the polymer film, $H_\perp$ is related to the plastic deformation mode of the lamellar stacks. On the other hand, H_{II} is concerned by the instant elastic recovery of the material [5]. In the drawn film, H_{II} is larger than $H_\perp$ after releasing of the load.

The indentation anisotropy, ΔH, is defined [1,16] as ;

$$\Delta H = 1 - (H_\perp/H_{II}) = 1 - (d_{II}/d_\perp)^2 \qquad (9.2)$$

The anisotropy is appeared by the orientation of the molecular axis, giving rise to a larger elastic recovery of the material in the chain direction. It has been shown that ΔH is a suitable parameter for measuring the preferred chain axis orientation [1,16]. Indeed, a linear empirical correlation has been found between ΔH and the optical birefringence Δn for injection-moulded oriented polyethylene [16].

In addition, the hardness of a polymeric material is well described by a parallel model of alternating amorphous and crystalline regions. Using the hardness values H_a and H_c of the both phases [16],

$$H = H_c\,\alpha_c + H_a\,(1-\alpha_c), \qquad (9.3)$$

where α_c is the volume degree of crystallinity (See Eq(4.5)).

Moreover, H_c is related to the crystalline lamellar thickness, L_c , through

$$H_c = H_c^{\infty} / (1+ b/L_c), \qquad (9.4)$$

where H_c^{∞} is the hardness of an infinitely thick crystal [16]. The value b is a parameter defined as:

$$b = 2\sigma_e/\Delta h, \qquad (9.5)$$

where σ_e being the surface free energy of the crystals and Δh being the energy for plastic deformation of the crystalline lamellae.

9.3 Comparative studies of PP by microhardness and X-ray

In chapter 5, we have explained the details about the PP textures by TSC. We have seen that PP is crystallized into the α (monoclinic) and the β (hexagonal) forms. In order to detect the mechanical properties of the two crystals, the oriented α and β textures were used for the microhardness measurement [7]. As seen in Fig. 5.5b (chapter5, pp54), the α and β crystals show a distinct separation by the transition line on the same film.

In the preliminary investigation, densities of the both crystals are measured to;

$\rho^{\alpha} = 0.913$ g/cm^3 for the α-phase texture, and

$\rho^{\beta} = 0.903$ g/cm^3 for the β-phase.

We take the values $\rho_c^{\alpha} = 0.940$ g/cm^3, $\rho_c^{\beta} = 0.939$ g/cm^3 and $\rho_a = 0.850$ g/cm^3, as the α and β crystalline densities and the amorphous density, respectively [10]. Followed by Eq.(4.5), α_c is calculated as $\alpha_c^{\alpha} = 0.721$ and $\alpha_c^{\beta} = 0.619$ for the α- and β-phases, respectively.

Microhardness was measured on the both phases at room temperature. The H value was derived according to Eq.(9.1) by the diagonal lengths measured from the residual indentation. Loads of 0.5 and 1 N were employed to eliminate the instant elastic contribution. A loading cycle of 0.1 min was used. As the region between the α- and β-phases on the sample surface is very sharp, indentations across the transition region could not be made. About 100 indentations were made on the surface of both phases to characterize the values of H^{α} and H^{β}. The accuracy of H for each phase is believed to lie within 1%.

The results collected in Table 9.1 show that the H decreases from 111MPa to 90MPa when passing from the α to β-phase texture. This hardness decrease is partially connected with the density reduction and, consequently, with the crystallinity decrease. While the ΔH value of the α-phase is low (3%), it increases to 20% in the β-phase. This difference is associated with a rise in the number of tie molecules connecting better oriented crystals in the β-phase.

In Fig.5.6b (chapter 5, pp55), the SAXS pattern of the oriented β-phase shows typical 2-point pattern. The precise layer structure has been explained in Fig.7.2 (chapter 7, pp99). The results confirms that β-lamellae are well oriented along the growth direction. On the other hand, the SAXS pattern of the α-phase shows 4-point pattern. The existence of the cross-hatched lamellae in the α-phase (chapter 5, pp55 and pp67-68) is the part of the reason of the low ΔH. In Table 9.1, the results of H and ΔH values indicate clear separation of the α- to β-phase of PP.

According to Eq (9.3), we can write for the both phases:

$$H^{\alpha} = H_c^{\alpha}\, \alpha_c^{\alpha} + (1 - \alpha_c^{\alpha})\, H_a \quad \ldots\ldots (9.6)$$

$$H^{\beta} = H_c^{\beta}\, \alpha_c^{\beta} + (1 - \alpha_c^{\beta})\, H_a \quad \ldots\ldots (9.7)$$

A value of $H_a \approx 30$MPa for amorphous phase of isotactic PP at room temperature has been reported [12]. Using the above equations, values of the crystalline hardness are calculated to $H_c^{\alpha} = 143$MPa and $H_c^{\beta} = 119$MPa for the α- and β- crystalline phases, respectively.

In conclusion, microhardness is shown to be a technique capable of detecting polymorphic changes in polymers. The results of microhardness confirms that additive contribution of the independent phase components H_c^{α}, H_c^{β} and H_a.

Table 9.1 Microhardness, indentation anisotropy, crystallinity and crystal hardness for the α and β- PP by TSC.

Sample	H (MPa)	ΔH	α_c	H_c (MPa)
α-phase	111	3	0.721	143
β-phase	90	19	0.619	119

9.4 Comparative studies of PET by microhardness and X-ray

The methods of preparing PET sample and the details of its crystallization process studied by X-ray diffraction have been presented in chapter 4 (pp 30-31) [9]. A brief description of the sample is that the amorphous PET was drawn at room temperature, and the drawn sample was then annealed in the temperature range of T_a = 50 - 250°C with annealing time t_a=10, 10^2, 10^3 and 10^4s for microhardness studies. The procedure for measuring microhardness of the sample is similar to that of PP as described above. The example of the indentation patterns is shown in Fig.9.2. Due to molecular orientation by the mechanical drawing, the indentation pattern of the PET sample has anisotropic diagonal lengths as illustrated in Fig.9.1(b) and 9.2(b).

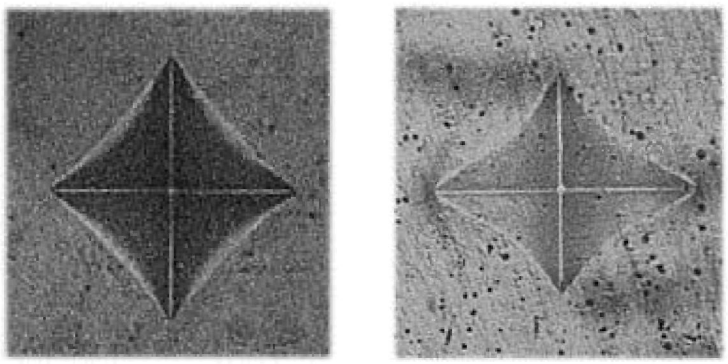

(a) (b)

Fig. 9.2 Indentation patterns of (a) isotropic PET and (b) oriented PET [17]

In Fig.9.3, the $H_{\parallel}$ and $H_{\perp}$ values are compared as a function of the annealing temperature with different annealing times. The hardness value for the cold-drawn sample before annealing (T_a=20°C) appears at $H_{\parallel}$=125MPa and $H_{\perp}$=75MPa. At T_a > 70 °C, both values increase with development of the triclinic crystal. The $H_{\parallel}$ values are higher than the $H_{\perp}$ values for all the series of the annealed times (t_a = 10, 10^2, 10^3 and 10^4 s).

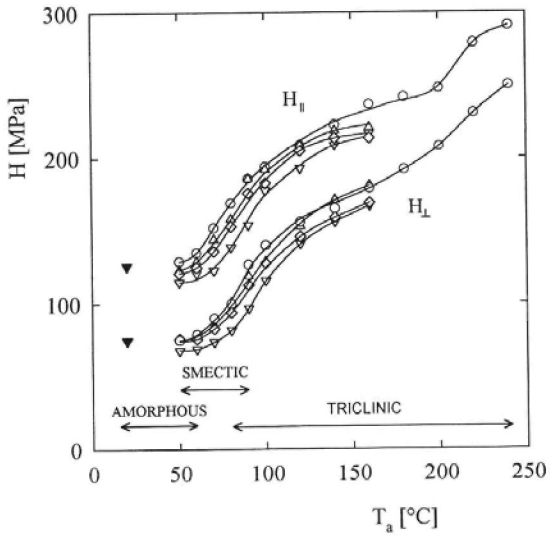

Fig. 9.3 $H_{\parallel}$ and $H_{\perp}$ as a function of the annealing temperature for different annealing times: ∇: t_a = 10 s; ◊: t_a = 10^2 s; Δ: t_a = 10^3 s; ○: t_a = 10^4 s; ▼: cold-drawn sample without annealing.[9]

Figure 9.4 illustrates the variation of the indentation anisotropy (ΔH) for the series of PET samples as a function of the annealing temperature (T_a) at different annealing time t_a. From investigations of other oriented polymer samples [14 -16], ΔH is known to correlate to the longitudinal elastic modulus. At the low annealing temperatures (T_a< 70°C), ΔH shows ~40%, which is an extremely high anisotropy value compared to other polymer samples. Above 70°C, close to the glass transition (T_g) of PET, ΔH rapidly decreases to less than 20%. In our structural investigation in chapter 4, the change in ΔH is closely related to the development of the triclinic lamellae.

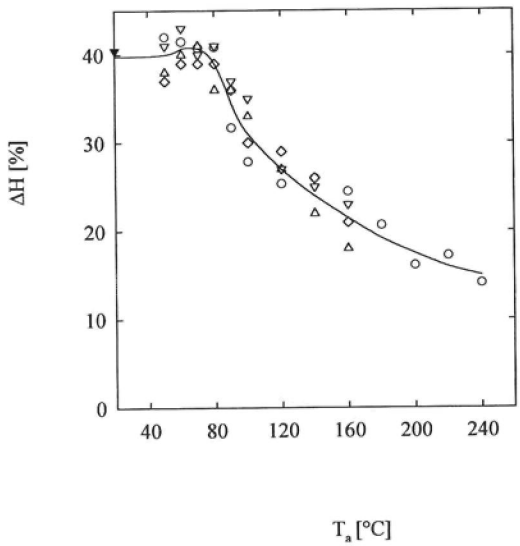

Fig. 9.4 ΔH as a function of the annealing temperature for different annealing times. Symbols are same as in Fig. 9.3.[9]

The rapid decrease of ΔH for $T_a > 70^oC$ is connected with the concurrent decrease in the elastic properties of the layer structure. In chapter 4, development of the layers are studied by the cold drawn PET. It was shown that after a change from nematic (20 °C) to smectic (60°C), the precursor state appears at 70°C and the triclinic structure develops above 80°C [9]. During the triclinic crystallization, SAXS indicates the typical 4-point pattern by inclined layers (Fig.4.6, pp36).

The ΔH decrease could be related to the development of the lamellar structure starting at 70°C. In the amorphous layers, the local molecular orientation will be relaxed by the development of the layer structure. As a result of the concentration of the unoriented molecules, the elastic recovery in the chain direction will decrease in the amorphous layers. The observed decrease in ΔH is closely related to the relaxation of the molecular orientation in the amorphous layers.

In the cold-drawn PET, the crystallinity α_c continuously increases with T_a. The observed α_c and $H_\perp$ values are listed in Table 9.1. For $T_a < 100^oC$, $H_\perp$ increases by the densification of smectic domains. The $H_\perp$ increase with $T_a \geq 100$ °C could be explained development of the triclinic crystal.

According to Eq (9.3), the hardness increases with α_c. However, H_c is known to vary with L_c according to Eq (9.4). Then, Eq (9.3) is rewritten as:

$$H_\perp = [(H_c)_\perp - (H_a)_\perp]\,\alpha_c + (H_a)_\perp \quad \text{..... (9.8)}$$

The process of the calculation by Eq.(9.8) is shown by the dotted line in Fig.9.5. If we approximate the $(H_a)_\perp$ value to the hardness of the cold drawn sample [$\alpha_c = 0$, $(H_a^{glass})_\perp$ = 75MPa], then the $(H_c)_\perp$ becomes 325 MPa for all samples annealed at $T_a \geq 140$ °C ($\alpha_c \geq 0.35$).

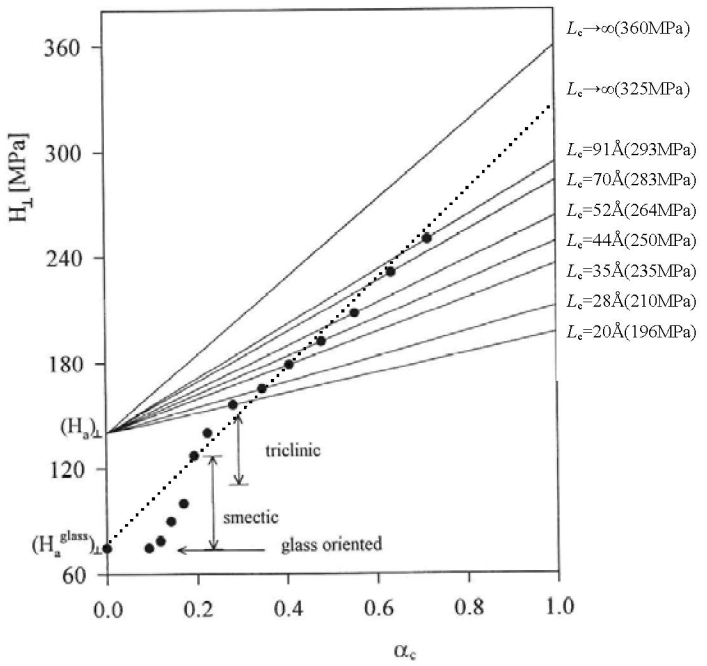

Fig. 9.5 $H_\perp$ variation with α_c for the samples annealed during 10^4 s. The straight lines followed by Eq (9.11) with $(H_a)_\perp$ = 140 MPa.[9]

However, in the previous indentation experiments, PET microfibrils, a very high degree of crystallinity (α_c ~1) and nearly extended chains ($L_c \rightarrow \infty$), give an $H_\perp$ value of 360MPa [16]. Thus, the obtained value of $(H_c^\infty)_\perp$ ~ 325MPa seems rather low. Moreover, $(H_c)_\perp$ values must be changed with increasing L_c.

From these considerations, the hardness of the amorphous constrained regions within the crystals should be higher than that of a completely amorphous oriented sample. We suppose the higher $(H_a)_\perp$ value of 140MPa, which is the hardness of the sample annealed at T_a =100 °C (α_c=0.22). Assuming a value of $(H_a)_\perp$ = 140MPa, it is possible to draw a family of straight lines in Fig. 9.5. Then, the extrapolation at α_c= 1 gives the crystal hardness $(H_c)_\perp$ for each L_c value. Following Eq.(9.4), b values are calculated by each L_c value using $(H_c^\infty)_\perp$ =360MPa. The b values are almost constant during increasing α_c. The results of $(H_c)_\perp$ and b are summarized in Table 9.1.

Table 9.1. lamellar spacing L and microhardness $H_\perp$ of the cold drawn PET annealed at temperature T_a (t_a = 10^4 s) [9].

T_a (°C)	L (Å)	α_c	L_c (Å)	$H_\perp$ (MPa)	$(H_c)_\perp$ (MPa)	b (Å)
100	55	0.22	14	140	-	-
120	62	0.28	20	157	196	16
140	70	0.35	28	165	210	19
160	77	0.41	35	180	235	20
180	82	0.48	44	192	250	19
200	88	0.55	52	208	264	19
220	106	0.63	70	231	283	19
240	126	0.72	91	250	293	21

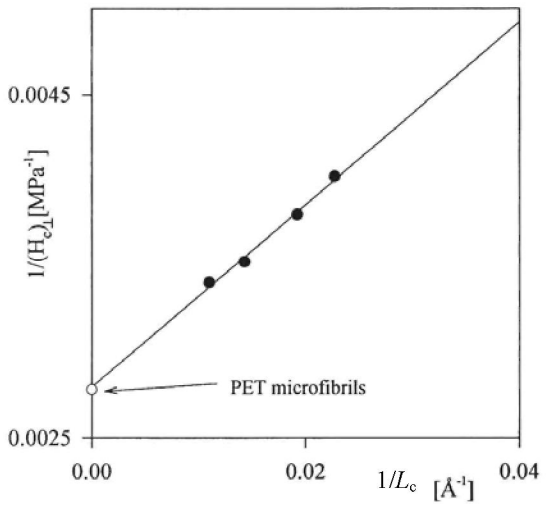

Fig. 9.6 Plot of $1/(H_c)_\perp$ as function of $1/L_c$. Open circle: $H_\perp$ of highly crystalline chain-extended PET microfibrils.

To confirm the ultimate value $(H_c^{\infty})_{\perp}$, we plot $1/(H_c)_{\perp}$ values in Fig.9.6. According to Eq (9.4), a polt of $1/(H_c)_{\perp}$ values versus $1/L_c$ values will fit into a straight line (if b is constant) of slope $b/(H_c)_{\perp}$ and ordinate intercept $1/(H_c)_{\perp}$. Figure 9.6 illustrates the variation of $1/(H_c)_{\perp}$ for samples annealed at $T_a \geq 180°C$ ($\alpha_c = 0.5$). In the derivation of the $(H_c)_{\perp}$ values, a value of $(H_a)_{\perp}$ = 140MPa was used. The data in Fig 9.6 fit to a straight line. The intercept gives $(H_c^{\infty})_{\perp}$ = 358MPa, which is in excellent agreement with $H_{\perp}$ of highly crystalline chain-extended PET microfibrils (= 360 MPa) [16]. Lower $(H_a)_{\perp}$ values would yield higher intercepts and hence, smaller $(H_c^{\infty})_{\perp}$ values.

The above analysis suggests that the hardness value for the amorphous constrained regions ($(H_a)_{\perp} \sim$ 140MPa) is higher than that of the starting oriented amorphous material. The fact is also explained in the structural analysis in chapter 4. As shown in Figs. 4.10, 4.11, 4.13, the molecules in the amorphous layer are highly oriented in the cold-drawn PET. The difference of the hardness between the glassy amorphous state (75MPa) and triclinic amorphous layer (140MPa) is originated from the molecular orientation.

The microhardness experiments give the finer understanding of polymer morphology. The cooperation with structural and mechanical observation has been made by other polymers in our laboratory. The examples of the works are listed in the references [18-28].

References

1. F. J. Baltá Calleja and S. Fakirov, in *"Microhardness of Polymers"*, Cambridge University Press, 2000.
2. D. Tabor, in *"The hardness of Metals"*, Oxford C. Press, 1951.
3. H. O'Neill, in *"Hardness Measurement of Metals and Alloys"*, Chapman & Hall, 1967.
4. F. J. Baltá Calleja, *Adv. Polym. Sci.* **66**, 117, (1985).
5. Y. Deslandes, E. Alva Rosa, F. Brisse and T. Meneghini, *J. Mater. Sci.*, **26**, 2769, (1991).
6. F. J. Baltá Calleja, *Trends Polym. Sci.*, **2**, 419 (1994).
7. F. J. Baltá Calleja, J. Martinez Salazar and T. Asano, *J. Mater. Sci. Lett.*, **7**, 165 (1988).
8. F. J. Baltá Calleja and S. Fakirov, *Trends Polym. Sci.*, **5**, 246 (1997).
9. T. Asano, F. J. Baltá Calleja, A. Flores, M. Tanigaki, M. F. Mina, C. Sawatari, H. Itagaki, H. Takahashi and I. Hatta, *Polymer*, **40**, 6475 (1999).
10. G. Brandrup and E. H. Immergut, *"Polymer Handbook"*, 2nd Edn., Wiley, Interscience, New York (1975).
11. F. J. Baltá Calleja, J. Martínez Salazar, H. Cacovic and J Loboda-Cacovic, *J. Mater. Sci.*, **16**, 739 (1981).
12. J. Martinez Salazar, G. M. Gracia Tijero and F. J. Baltá Calleja, *J. Mater Sci.* **23**, 862 (1988)
13. F. J. Baltá Calleja, *Adv. Polym. Sci.*, **66**, 117 (1985).
14. A. Fichera and R. Zanneti, *Makromol. Chem.* **176**, 1885 (1975).
15. D. R. Rueda, F. J. Baltá Calleja, J. Gracía Peña, I. M. Ward and A. Richerdson, *J. Mater. Sci.* **19**, 2615 (1984).
16. M. Krumova, S. Fakirov, F. J. Baltá Calleja, and M. Evstatiev, *J. Mater. Sci.* **33**, (1998).

17. Private communications from S. Henning and F. J. Baltá Calleja (2006)
18. F. J. Baltá Calleja, C. Santa Cruz, C. Sawatari and T. Asano, *Macromolecules*, **23**,5352, (1990)
19. C. Santa Cruz, F. J. Baltá Calleja, H.G. Zachmann, N. Stribeck and T. Asano, *J. Polym. Sci.*, **29**, 819-824 (1991)
20. C. Santa Cruz, F. J. Baltá Calleja, T. Asano and I.M. Ward, *Phil. Mag.*, **68**, 209-224 (1993)
21. F. J. Baltá Calleja, C. Santa Cruz and T. Asano, *J. Polym. Sci.*, **31**, 557-565 (1993)
22. F. J. Baltá Calleja, L. Giri, T. Asano and T. Yoshida, *Rep. Fac. Sci. Shizuoka Univ.*, **28**, 53-60, (1994)
23. F. J. Baltá Calleja, L. Giri, T. Asano, T. Mieno, A. Sakurai, M. Ohnuma and C. Sawatari, *J. Mater. Sci.*, **31**, 5153-5157 (1996)
24. T. Yoshida, T. Asano, N. Miyashita, M. Matsu-ura, J. Kitabatake, I. Hatanaka, K. Seri, F. J. Baltá Calleja and L. Giri, *J. Macromol. Sci. Phys.*, **B36**, 789-798 (1997)
25. T. Asano, F. J. Baltá Calleja, L. Giri, T. Yoshida, N. Miyashita, M. Matsu-ura, J. Kitabatake, I. Hatanaka, K. Seri, *J. Macromol. Sci. Phys.*, **B36**, 799-812 (1997).
26. A. Flores, F. J. Baltá Calleja and T. Asano, *J. Appl. Phys*. **90**, 6006-6010, (2001).
27. M. F. Mina, M. E. Haque, F. J. Baltá Calleja, T. Asano, M. M. Alam, *J. Macromol. Sci., PartB-Phys*. **B43**, No5, 1005-1014 (2004)
28. M. F. Mina, F. Ania, F. J. Baltá Calleja and T. Asano, *J. Appl. Polym. Sci.*, **91**, 205-210 (2003)